NeuroImage: Clinical 28 (2020) 102413

Contents lists available at ScienceDirect

NeuroImage: Clinical

journal homepage: www.elsevier.com/locate/ynicl

Cognitively supernormal older adults maintain a unique structural connectome that is resistant to Alzheimer's pathology

Quanjing Chen[a,b,*], Timothy M. Baran[c,d], Brian Rooks[e], M. Kerry O'Banion[f], Mark Mapstone[g], Zhengwu Zhang[e], Feng Lin[a,b,f,h,i,*], for the Alzheimer's Disease Neuroimaging Initiative[1]

[a] Elaine C. Hubbard Center for Nursing Research on Aging, School of Nursing, University of Rochester Medical Center, United States
[b] Department of Psychiatry, School of Medicine and Dentistry, University of Rochester Medical Center, United States
[c] Department of Imaging Sciences, School of Medicine and Dentistry, University of Rochester Medical Center, United States
[d] Department of Biomedical Engineering, University of Rochester, United States
[e] Department of Biostatistics and Computational Biology, School of Medicine and Dentistry, University of Rochester Medical Center, United States
[f] Department of Neuroscience, School of Medicine and Dentistry, University of Rochester Medical Center, United States
[g] Department of Neurology, University of California-Irvine, United States
[h] Department of Neurology, School of Medicine and Dentistry, University of Rochester Medical Center, United States
[i] Department of Brain and Cognitive Sciences, University of Rochester, United States

ARTICLE INFO

Keywords:
Supernormals
Longitudinal design
White matter structural connectome
AD pathology
Mild cognitive impairment

ABSTRACT

Studying older adults with excellent cognitive capacities (*Supernormals*) provides a unique opportunity for identifying factors related to cognitive success – a critical topic across lifespan. There is a limited understanding of Supernormals' neural substrates, especially whether any of them attends shaping and supporting superior cognitive function or confer resistance to age-related neurodegeneration such as Alzheimer's disease (AD). Here, applying a state-of-the-art diffusion imaging processing pipeline and finite mixture modelling, we longitudinally examine the structural connectome of *Supernormals*. We find a unique structural connectome, containing the connections between frontal, cingulate, parietal, temporal, and subcortical regions in the same hemisphere that remains stable over time in Supernormals, relatively to typical agers. The connectome significantly classifies positive vs. negative AD pathology at 72% accuracy in a new sample mixing Supernormals, typical agers, and AD risk [amnestic mild cognitive impairment (aMCI)] subjects. Among this connectome, the mean diffusivity of the connection between right isthmus cingulate cortex and right precuneus most robustly contributes to predicting AD pathology across samples. The mean diffusivity of this connection links negatively to global cognition in those Supernormals with positive AD pathology. But this relationship does not exist in typical agers or aMCI. Our data suggest the presence of a structural connectome supporting cognitive success. Cingulate to precuneus white matter integrity may be useful as a structural marker for monitoring neurodegeneration and may provide critical information for understanding how some older adults maintain or excel cognitively in light of significant AD pathology.

1. Introduction

Normal aging is typically characterized by cognitive decline (Park & Reuter-Lorenz 2009), particularly in processing speed and memory domains (Brickman & Stern 2009). Typical memory decline is most evident on tasks of episodic memory (Rönnlund et al 2005), with multiple studies showing greatest age-related declines after age 60 (Nyberg & Pudas 2019). Despite this, variability in cognitive performance, either across cognitive domains or within cognitive domains across time, also tends to increase with advancing age (Frias et al 2007). This is perhaps most evident for individuals who do not exhibit the expected reduction in episodic memory with advanced age. Older adults with excellent cognition, especially episodic memory, often defined as superior to age-matched counterparts (*Supernormals*) (Lin et al

* Corresponding author at: University of Rochester Medical Center, 430 Elmwood Ave, Rochester, NY 14642, United States.
E-mail addresses: Quanjing_Chen@URMC.Rochester.edu (Q. Chen), vankee_lin@urmc.rochester.edu (F. Lin).

[1] Data used in preparation of this article were obtained from the Alzheimer's Disease Neuroimaging Initiative (ADNI) database (adni.loni.usc.edu). As such, the investigators within the ADNI contributed to the design and implementation of ADNI and/or provided data but did not participate in analysis or writing of this report. A complete listing of ADNI investigators can be found at: http://adni.loni.usc.edu/wp-content/uploads/how_to_apply/ADNI_Acknowledgement_List.pdf.

https://doi.org/10.1016/j.nicl.2020.102413
Received 9 April 2020; Received in revised form 30 August 2020; Accepted 2 September 2020
Available online 08 September 2020

2017a, Mapstone et al 2017) or equivalent to that of younger adults (*Superagers*) (Harrison et al 2018, Rogalski et al 2013, Sun et al 2016) are a powerful model to study cognitive resilience. We choose to use the Supernormal definition in the current study to minimize cohort differences such as educational access and exposure to technology that could affect comparison with younger cohorts. For many Supernormals, superior cognitive performance is maintained over time (Lin et al 2017b), indicating that this effect is distinct, and not due simply to decline that remains above a normal cutoff (Fiocco & Yaffe 2010). There is a growing emphasis in examining biological models of successful cognitive aging in order to understand longevity (Nyberg & Pudas 2019, Olshansky 2018). We study these older adults with excellent cognition in order to identify and understand neural mechanisms of cognitive success that are resistant to the effects of aging and support a healthy lifespan (a.k.a. health span (Olshansky 2018, Seals et al 2016)).

Supernormals seem to display unique brain functional and structural profiles that differ from age-matched cognitively normative older or younger adults. In terms of brain function, Supernormals preserve stable function of posterior brain regions, the ventral pathway of the prefrontal cortex, and selected networks (e.g., default mode network, salience network), and engage bilateral hemispheres (Persson et al 2011, Wang et al 2017, Zhang et al 2020). In terms of brain structure, Supernormals show preserved cortical thickness or volume of critical nodes in the default mode network and salience network (Gefen et al 2015, Harrison et al 2012, Rogalski et al 2013, Sun et al 2016). It is evident that white matter (WM) integrity plays a critical role in supporting and shaping brain function (Monje 2018). Furthermore, variability in WM integrity has been related to innate cognitive ability (Schmithorst et al 2005), age-related cognitive decline (Voineskos et al 2012), and neurodegenerative diseases (Medina et al 2006). Cumulative evidence suggests that AD is a connectome disease, and tau spreads via neuronal connections (Acosta-Cabronero et al., 2010; Dai & He, 2014; Damoiseaux et al., 2009; Delbeuck et al., 2003; Rose et al., 2000). Deficits in WM connectivity are associated with AD pathology across cognitive stages, from intact cognition, to MCI and AD (Kim et al 2019, Lim et al 2014, Mayo et al 2017). Synthesizing these separate lines of evidence, we suspect that the longitudinal integrity of WM connectivity is important for supporting successful aging and can predict AD related outcomes in Supernormals."

Here, applying a state-of-the-art diffusion imaging processing pipeline (Zhang et al 2018), we examined the structural connectome in cognitively superior older adults (*Supernormals, SN*) that we previously identified in the ADNI cohort (Lin et al 2017a, Lin et al 2017b) over a 2-year period. This longitudinal design enabled us to test whether Supernormals maintain a unique structural connectome that remains stable over time. In addition, since Alzheimer's disease (AD) is the most common neurodegenerative disease, we tested whether WM integrity of the supernormal structural connectome predicts AD-related outcomes such as AD pathology, neurodegeneration and global cognition over 2 years.

2. Methods

2.1. Data Source

Data used in the preparation of this article were obtained from the Alzheimer's Disease Neuroimaging Initiative (ADNI) database (adni.loni.usc.edu). The ADNI was launched in 2003 as a public–private partnership, led by Principal Investigator Michael W. Weiner, MD. The primary goal of ADNI has been to test whether serial magnetic resonance imaging (MRI), positron emission tomography (PET), other biological markers, and clinical and neuropsychological assessment can be combined to measure the progression of mild cognitive impairment (MCI) and early Alzheimer's disease (AD). To reduce site related errors, ADNI group made strict attempts to standardize patient recruitment and imaging protocols across the different sites. ADNI collects diffusion-weighted images at 14 sites arcoss North America, all using the same scanner manufacturer (General Electric), magnetic field strength (3T) and protocol, including the same voxel size and the number of gradient directions. The ADNI group also did rigorous quality control and assurance of scanners. Each exam underwent a quality control evaluation at the Mayo Clinic (Rochester, MN, USA). Quality control included inspection of each incoming image file for protocol compliance, clinically significant medical abnormalities, and image quality (Jack et al 2008).

2.2. Participants

All subjects in this study were from ADNI GO and ADNI2 where DTI data were collected using 3T GE scanners. We developed and validated the "Supernormal structural connectome" in three steps: identification of a "Supernormal structural connectome", internal validation, and external validation in prodromal AD.

For the first step, we identified a group of older adults without cognitive impairment (referred to as "Normative" afterwards) [n = 48, including 24 Supernormals (SN_I) and 24 cognitively normative controls (AC_I) with matched age and education] who had DTI data at 2 time points (2 years apart) from our previous dataset (including 354 older adults free of dementia/aMCI or major psychiatric disorders over the course of participation in ADNIGO and ADNI2)(Lin et al 2017b). The identification of Supernormals and cognitively normative controls was based on 5-year trajectories of composite episodic memory (EM) and executive function (EF) scores as described previously (Lin et al 2017b). In previous analysis, we applied finite mixture models to examine 5-year trajectories of EM and EF standardized composite scores. Three latent classes were generated. Supernormal showed significantly different intercept and slope in EM, as well as different slope in EF, from the other 2 classes. In the current study, SN were selected from the supernormal class while AC were from the other 2 classes. According to EF and EM cut-off scores (Crane et al., 2012; Gibbons et al., 2012), a score above 0 indicates normal cognition and SD = 1. In the current study, SN and AC are all above 0. These SN_I subjects had baseline EM and EF mean z-scores of 1.60 ± 0.57 and 1.12 ± 0.69, respectively, compared to 0.95 ± 0.49 and 0.53 ± 0.59 for AC_I. These are approximately 1 standard deviation above the overall normal population mean, indicating that this SN_I group is at or above 84% of the population, assuming cognitive scores are normally distributed. SN and AC also significantly differed in EM and EF across internal and external validation samples, controlled for age, sex and education (see Table 1). Among SN_I and AC_I, we selected participants who had DTI data, CSF Aβ and pTau data, FDG-PET or global cognition (MOCA) from the same 6-month window at 2 time points (2 years parts) for internal validation (step 2). MOCA scores significantly differed between SN_I and AC_I. There was no significant difference between SN_I and AC_I in Aβ/pTau or composite FDG-PET score at either time point (see Table 1).

For the last step (external validation), we identified a different set of cognitively non-impaired (n = 24, including 10 SN_E and 14 AC_E) and aMCI (a group at high risk for AD, n = 33) participants who had DTI data at one time point as well as CSF Aβ and pTau data from the same 6-month window. The diagnoses of aMCI were made by a psychiatrist or neurologist at each study site and reviewed by a Central Review Committee based on serial neuropsychological tests (details in Fig. 1). The three groups (SN_E, AC_E and aMCI) significantly differed in cognitive performance and AD pathology, controlled for age, sex and education (see Table 1).

2.3. Data Acquisition

All participants underwent whole-brain MRI scanning on 3 T GE scanners. Diffusion-weighted images (DWI) were collected with the following parameters: matrix size = 256 × 256 mm; flip angle = 90°; slice thickness = 2.7 mm; 41 diffusion-weighted images (b = 1000 s/mm^2) and 5 non-diffusion-weighted b0 image. T1-weighted spoiled

Table 1
Sample characteristics.

Identification of "Supernormal structural connectome" and Internal validation			SN_I (N = 24)		AC_I (N = 24)		T, F or χ^2 test, df1, df2, (P)	
Age baseline, Mean (SD)			72.56	(5.54)	72.71	(3.23)	−0.11, 46	(0.91)
Male, N (%)			8	(33)	9	(38)	0.01, 1	(0.76)
Education, Mean (SD)			16.96	(2.73)	15.67	(2.60)	1.68, 46	(0.10)
APOE4 carrier, N (%)			6	(25)	10	(41)	1.50, 1	(0.22)
EM baseline, Mean (SD)			1.60	(0.57)	0.95	(0.49)	**15.79, 1, 43**	**(< 0.001)** [ξ]
EM year 3 Mean (SD)			1.77	(0.49)	0.80	(0.48)	**41.52, 1, 43**	**(< 0.001)** [ξ]
EF baseline, Mean (SD)			1.12	(0.69)	0.53	(0.59)	**7.64, 1, 43**	**(0.008)** [ξ]
EF year 3, Mean (SD)			1.46	(0.55)	0.54	(0.63)	**27.87, 1, 43**	**(< 0.001)** [ξ]
MOCA baseline, Mean (SD)			27.04	(1.88)	25.21	(1.56)	**12.87, 1, 43**	**(0.001)** [ξ]
MOCA year 3, Mean (SD)			27.42	(2.15)	25.00	(2.00), n = 23	**11.87, 1, 42**	**(0.001)** [ξ]
CSF Aβ/pTau ratio baseline, Mean (SD)			4.06	(0.60), n = 18	4.20	(0.60), n = 20	0.39, 1, 33	(0.535) [ξ]
CSF Aβ/pTau ratio year 3, Mean (SD)			3.86	(0.63), n = 10	3.85	(0.75), n = 10	0.03, 1, 15	(0.818) [ξ]
positive AD pathology baseline, N (%)			6	(33), n = 18	6	(30), n = 20	0.05, 1	(0.825)
positive AD pathology year 3, N (%)			5	(50), n = 10	5	(50), n = 10	0, 1	(1)
Composite FDG-PET ROI baseline, Mean (SD)			1.37	(0.10)	1.31	(0.12), n = 23	2.29, 1, 42	(0.138) [ξ]
Composite FDG-PET ROI year 3, Mean (SD)			1.31	(0.07), n = 11	1.27	(0.09), n = 12	0.68, 1, 18	(0.419) [ξ]
External validation	SN_E (N = 10)		AC_E (N = 14)		aMCI (N = 33)		T, F or χ^2 test, df1, df2, (P)	
Age baseline, Mean (SD)	74.81	(10.77)	76.00	(6.88)	72.48	(5.78)	1.34, 2, 54	(0.27)
Male, N (%)	6	(60)	7	(50)	21	(64)	0.76, 2	(0.68)
Education, Mean (SD)	16.10	(2.84)	16.57	(2.73)	15.97	(2.89)	0.22, 2, 54	(0.80)
APOE4 carrier, N (%)	2	(20)[a]	5	(36)[a]	27	(82)[b]	**16.60, 2**	**(< 0.001)**
EM, Mean (SD)	1.17	(0.29) [a]	0.72	(0.61) [b]	−0.40	(0.60) [c]	**37.74, 2, 51**	**(< 0.001)**[ξ]
EF, Mean (SD)	1.14	(1.00) [a]	0.30	(0.87) [b]	0.05	(0.91) [b], n = 32	**7.73 2, 50**	**(< 0.001)**[ξ]
MOCA, Mean (SD)	25.67	(2.69) [a], n = 9	24.92	(2.78) [a]	21.13	(2.55) [b], n = 32	**18.28, 2, 49**	**(< 0.001)**[ξ]
CSF Aβ/pTau ratio, Mean (SD)	4.28	(0.48) [a]	4.11	(0.59) [a]	3.22	(0.65) [b]	**19.81, 2, 51**	**(< 0.001)**[ξ]
positive AD pathology, N (%)	2	(20) [a]	5	(36) [a]	27	(82) [b]	**16.60, 2**	**(< 0.001)**

Note: SN_I, Supernormals; AC_I, average-ager controls (for Identification of " Supernormal structural connectome" and Internal validation); SN_E, Supernormals; AC_E, average-ager controls (for External validation); aMCI, amnesic mild cognitive impairment; APOE4, apolipoprotein E ε4; SD, standard deviation; CSF, Cerebrospinal fluid; Aβ, Beta-amyloid-(1–42); pTau, phosphorylated tau ;FDG, fluorodeoxyglucose; EM, episodic memory; EF, executive function; MOCA, Montreal Cognitive Assessment. Aβ/pTau ratio was log transformed because it did not have a normal distribution. [ξ] Controlled for age, sex and education. [a, b, c] represents the post-hoc comparison difference from the F-test. Bold values indicate $P < 0.05$.

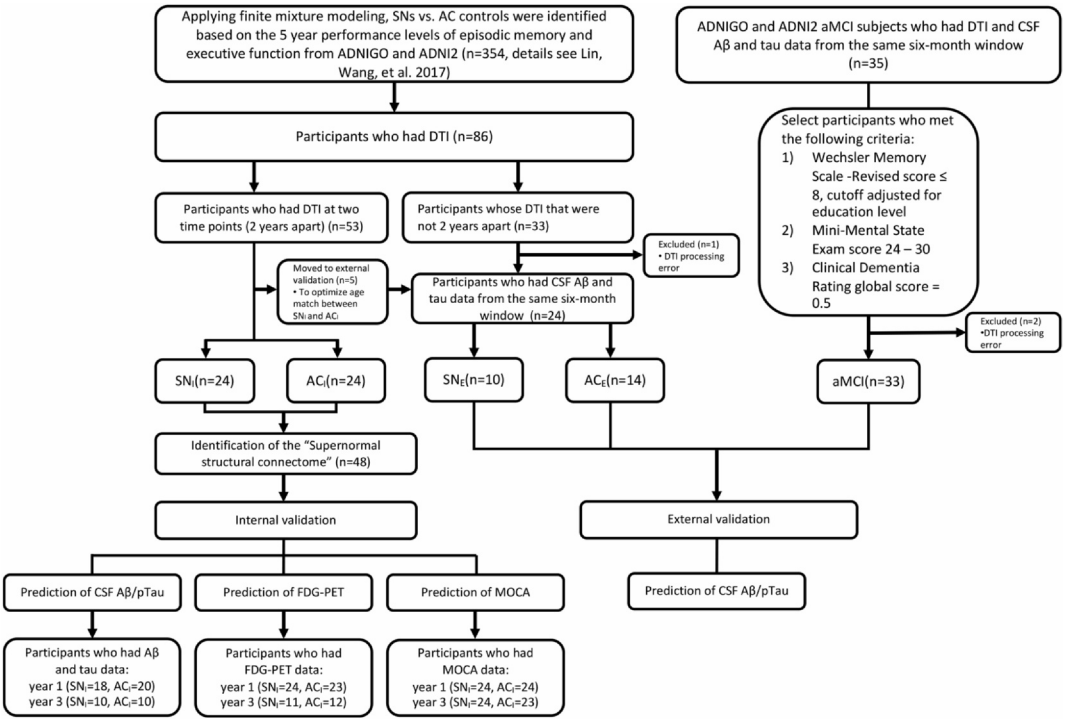

Fig. 1. Sample selection flow chart. Note. DTI, diffusion tensor imaging; aMCI, amnestic mild cognitive impairment; SN, Supernormals; AC, average-ager controls; I, for Identification of "Supernormal structural connectome" and Internal validation; E, External validation.

gradient recalled echo sequences were acquired in the same scanning session (TR = 7.0–7.7 ms, TE = 2.8–3.2, TI = 400 ms, matrix size = 256 × 256 mm, flip angle = 11°, resolution 1.02 × 1.02 mm, slice thickness = 1.20 mm). More details on ADNI protocols may be found at http://adni.loni.usc.edu/methods/documents/mri-protocols/.

2.4. Data Preprocessing

Each raw DWI image was aligned to the average b0 image using the FSL Eddy Correct tool version 6.0.1 (www.fmrib.ox.ac.uk/fsl) to correct for head motion and eddy current distortions. Non-brain tissue was removed using FSL's Brain Extraction Tool (Smith 2002). We then registered DWI images with the T1 anatomical images using Advanced Normalization Tools (ANTS; http://www.picsl.upenn.edu/ANTS/).

To extract brain connectome, we employed an established population-based structural connectome processing pipeline (Zhang et al 2018). First, we applied reproducible probabilistic tractography algorithm (Girard et al 2014, Maier-Hein et al 2017) to DWI data to generate streamlines across the whole brain. We used 0.2 mm step size and 25° angle threshold. The average seed number is about 10^5 voxels. Then, we used the Desikan atlas to define the Regions of Interest (ROIs) on T1 anatomical images. The brain of each participant was parcellated into 87 ROIs (68 cortical and 19 subcortical regions) with FreeSurfer. For each pair of ROIs, we extracted the streamlines connecting them. Then, we extracted 2 diffusion metrics from the streamlines to describe the connection: the mean of MD (mean diffusivity) and the mean of FA (fractional anisotropy). Another feature we extracted is CSA (connected surface area) which was proposed to reflect the amount of neurons connecting two regions (Zhang et al 2018). To calculate CSA, at each intersection between the surface of an ROI and a streamline, a small circle with fixed radius is drawn, and the total number of voxels covered by these circles is the CSA. CSA can be interpreted as the robustness of surface connection between two ROIs, and could be a metric for the sensitivity of the connection to neurodegeneration, either disease-related or due to normal aging. For reproducibility of metrics, the population-based structural connectome processing pipeline preserves the geometric information of streamlines and has been shown to extract much more reliable weighted brain networks, compared with a standard method from the literature (Zhang et al 2018).

2.5. Statistical analyses

We conducted a 3-step analysis. In the first step - Identification of "Supernormal structural connectome", we identified potential candidates for supernormal structural connectome. Numerous studies have shown that decreased FA and CSA, and increased MD are associated with AD and worse cognitive abilities (Bozzali & Cherubini 2007, Chua et al 2008, Nir et al 2013, Zhang et al 2019). Here, we expected to find a cluster which showed better WM integrity, indexed by higher FA, higher CSA, and lower MD, in SN than CN, to be the potential supernormal connectome map. In the second step - the internal validation, we tested whether the potential supernormal connectome map predicted AD related outcomes consistently across two time points in comparison to other clusters. If so, we considered it as the final supernormal connectome. Finally, the external validation validated the predictive ability of the supernormal connectome in an independent sample.

2.5.1. Identification of "Supernormal structural connectome"

Only the connections that could be traced in at least 80% of the total sample at both year 1 and year 3 were included. For each connection we calculated Z-scores for mean MD, mean FA, and CSA across all participants (SN_I + AC_I) and both years. A finite mixture modeling was conducted using R package, "FlexMix"(Leisch 2004). We used multivariate FMM to cluster connections based on the 3 white matter integrity measures at 2 time points for two groups. Clustering and estimation of the cluster parameters (intercepts, slopes, and variances) were performed simultaneously via the EM (Expectation-Maximization) algorithm. The six outcome variables of interest (MD, FA, CSA for SN_I and AC_I, respectively) of each connection and at each time point $t_j \in \{1, 3\}$ are modeled as observations drawn from a mixture of K six-dimensional multivariate normal distributions, with mixture component k assumed to have mean $\boldsymbol{\alpha}_k + \boldsymbol{\beta}_k t_j$ with $\boldsymbol{\alpha}_k, \boldsymbol{\beta}_k \in \boldsymbol{R}^6$, diagonal covariance matrix with variances $\sigma_{1k}^2, \cdots, \sigma_{6k}^2$, and mixture probability π_k for $k = 1, \cdots, K$.

Let $\boldsymbol{y}_{ij} \in \boldsymbol{R}^6$ denote the outcomes for connection i at time t_j, θ_k denote the set of parameters $\boldsymbol{\alpha}_k$, $\boldsymbol{\beta}_k$, $\sigma_{1k}^2, \cdots, \sigma_{6k}^2$ for mixture component k, and $f(.|\theta_k)$ denote the probability density function for mixture component k. After initializing $\theta_1, \cdots, \theta_K$ and the mixture probabilities $\pi_1, \cdots, \pi_K$, the EM algorithm iterates between two steps: the expectation step and the maximization step. The expectation step estimates the posterior probability that connection i belongs to cluster k given the estimated parameters via the formula

$$\hat{p}_{ik} = \frac{\pi_k \prod_{j=1}^{2} f(y_{ij}|t_{ij}, \theta_k)}{\sum_{l=1}^{K} \pi_l \prod_{j=1}^{2} f(y_{ij}|t_{ij}, \theta_l)}$$

for $k = 1, \cdots, K$. During the maximization step, mixture probabilities are estimated with the formula

$$\hat{\pi}_k = \frac{1}{n} \sum_{i=1}^{n} \hat{p}_{ik},$$

and estimates for $\theta_1, \cdots, \theta_K$ are obtained as the maximizers of the approximate complete-data log-likelihood

$$\sum_{k=1}^{K} \sum_{i=1}^{n} \hat{p}_{ik} \sum_{j=1}^{2} \log(f(y_{ij}|t_{ij}, \theta_k)).$$

The expectation and maximization steps are iterated in succession until convergence of the log-likelihood. The parameter estimates at convergence were used as the final estimates, and each connection assigned to the cluster with the maximum posterior probability of cluster membership. We trained the model with different initialization of number of clusters K (from 1 to 12). Then we compared Akaike Information Criterion (AIC), Bayesian Information Criterion (BIC) and log-likelihood as model selection criteria. Lower AIC and BIC and higher log-likelihood values indicate a better model fit.

2.5.2. Internal validation

The internal validation aimed to test the predictive power of the potential "Supernormal structural connectome" on AD related outcome, including AD pathology, neurodegeneration and global cognition, where FA, MD or CSA as predictor. As a comparison, we also tested the predictive power of the other five clusters.

AD pathology was measured by the ratio of Aβ and pTau, which was considered as the "AD signature" for which lower Aβ/pTau ratio indicated an increased burden of AD pathology. Aβ and pTau value were derived from CSF (Shaw et al 2009), and log transformed to approximate a normal distribution. Neurodegeneration was measured by FDG-PET, which was highly specific neurodegenerative imaging biomarker in AD. We generated a composite FDG score by averaging across five ROIs: right and left angular gyri, middle/inferior temporal gyrus, and bilateral posterior cingulate gyrus based on previous procedure (Jagust et al 2010). Global cognition was measured using the MOCA (Rossetti et al 2011). Here we chose MOCA as the cognitive measure since this measure was not included in the development of composite EM and EF scores that were used for characterizing Supernormals.

For each cluster, we used white matter integrity measures of each connectome at baseline as features (predictors), to predict AD pathology (CSF Aβ/pTau ratio), neurodegeneration (FDG-PET) and global cognition (MOCA) at both baseline (year 1) and 2-year follow-up (year 3) for the total sample (SN_I + AC_I). During regression, feature vectors were Z-transferred across subjects to ensure similarity of ranges for

feature values and comparable contribution of each feature to the final regression from both training and test sets (Chang & Lin 2011). Normalization was also performed on response variables. We employed support vector regression (SVR) with the linear kernel (Hsu and Lin, 2003) using Matlab. We chose linear kernel because it's easy to interpret the feature weights (e.g., which connection contributes most). We didn't use nonlinear kernels since it is difficult to interpret results and feature weights for SVM nonlinear kernels. Leave-one-out cross-validation was performed, i.e the classifier was trained on all except one subject on which testing was to be performed. This leave-one-out validation process was repeated for all subjects. After regression, we evaluated the results by correlating the observed and predicted outcomes. The correlation coefficient R was used to estimate goodness of fit for the model. To control the familywise error rate, we performed a Bonferroni correction, dividing the critical P value (α) by the number of clusters ($\alpha = 0.05/6 = 0.0083$).

2.5.3. External validation

Based on findings from the first two steps, the goal of external validation was to clinically validate the predictive power of the baseline MD of "Supernormal structural connectome" (cluster 5) on AD pathology in prodromal AD. Here we extracted MD of cluster 5 from a separate dataset (24 Normative (10 SN_E and 14 AC_E) and 33 aMCI). As with the internal validation, we used Leave-one-out cross-validation and SVR with the linear kernel to predict Aβ/pTau ratios. Besides, to ensure the clinical utility of the "Supernormal structural connectome", we also performed a classification (positive vs. negative AD pathology) with leave-one-out cross-validation and linear support vector machine (SVM). The cut-off for positive AD pathology was based on log-transformed CSF Aβ/pTau ratio < 3.82 (Hansson et al 2018). To evaluate the classification result, we did 5000 permutations that shuffled the class labels among the samples. The permutation p-value was reported as (number of permutation accuracy $>$ true accuracy) / number of permutations.

3. Results

3.1. Identification of the "Supernormal structural connectome"

Sample selection using ADNIGO and ADNI2, where diffusion imaging data are currently available, is described in Fig. 1. Sample characteristics are presented in Table 1. Data for developing the "Supernormal structural connectome" (labeled as internal/$_I$ sample) was derived from age- and education-matched SN_I ($n = 24$) and AC_I ($n = 24$). Using our diffusion imaging pipeline (Zhang et al 2018), we identified 1150 connections that existed in at least 80% of the total sample at both year 1 and year 3. We calculated Z-scores for mean FA, mean MD, and CSA across all subjects at the two time points. We applied finite mixture modeling (Ram & Grimm 2009), expecting a set of stable WM connections that are unique to Supernormals (see the **Method** section for more details). We analyzed data from all 3 Z-transformed WM integrity measures for 2 groups (SN_I vs. AC_I) at 2 time points (year 1 and year 3) to determine the longitudinal homogenous subsets of structural connections for the two groups, respectively. We trained models with different initialization of cluster numbers (from 1 to 12). The algorithm converged and stopped at a 6-cluster solution with the best model fit, indicated by the lowest AIC, lowest BIC and highest log-likelihood (Table 2). Thus, the 6-cluster model was used here. The 2-year trajectories across the WM measures for the 6 clusters in SN_I vs. AC_I are displayed in Fig. 2**A**. The connections within the 6 clusters are visualized in a two-dimensional plane (Fig. 2**B**). Synthesizing longitudinal characteristics of the 3 WM integrity measures between groups, Cluster 5 represents the subset of connections with better integrity for SN_I than AC_I characterized by initially **lower** and longitudinally stable MD and initially **higher** and longitudinally stable FA, and constantly **higher** CSA. Cluster 6 represents the subset of connections preferring AC_I than SN_I, characterized by initially **lower** and longitudinally **decreased** MD and initially **higher** and longitudinally **increased** FA, and initially **higher** and longitudinally stable CSA in AC_I. FA reflects the directionality of water diffusion through tissue with higher value associated with greater fiber integrity. AC_I show significantly **higher** FA than SN_I in Cluster 6, which is opposite to our expected Supernormal profile. To give a better view of distribution of these connections across the whole brain, we visualize Cluster 5 and Cluster 6 in a three-dimensional glass brain (Shen, 2017) (Fig. 3). Cluster 5 engages subcortical-cortical (except occipital) connections, dominantly within the same hemisphere, while Cluster 6 engages more interhemispheric connections in the occipital lobe. The other four clusters had overall **lower** MD in SN_I than AC_I, with inconsistent findings in FA and CSA. The intercept and slope results of the WM integrity measures for clusters are presented in Table 3. Based on these findings, we consider Cluster 5 a *potential* "Supernormal structural connectome".

3.2. Internal validation: Predictive values of the "Supernormal structural connectome" for AD-related outcomes

For each cluster, we examined the predictive value of the baseline WM integrity measures (FA, MD, or CSA) for AD pathology (CSF Aβ/pTau ratio), neurodegeneration (FDG-PET), or global cognition (MOCA) at two time points for the total sample ($SN_I + AC_I$). We considered a cluster for which an integrity measure can consistently predict an outcome across two time points, to be the *final* supernormal structural connectome. Here we use linear support vector regression (SVR) and leave-one-out cross validation for each cluster, taking individual connectome integrity values as features to predict individual outcomes in year 1 and year 3, respectively. The results are displayed in Fig. 4. We found baseline MD extracted from Cluster 5 significantly predicted Aβ/pTau ratio at both year 1 ($R = 0.645$, $P < 0.001$, significant with Bonferroni correction) and year 3 ($R = 0.584$, $P = 0.007$, significant with Bonferroni correction). Fig. 5**A** shows the prediction of Aβ/pTau ratio in year 1 and year 3 using baseline MD from Cluster 5 for internal validation. Fig. 5**B** displays the top 30% features (connections) with the largest coefficients in absolute value in SVR in year 1 or year 3 that predict Aβ/pTau ratio.

We evaluated the independent contribution of the WM baseline MD from Cluster 5 in predicting AD-related pathology, compared to demographic factors. We compared prediction accuracy in two modeling strategies, namely a full model and a baseline model. For the baseline model, we used only selective demographic characteristics (i.e., age, sex and education) as predictors. For the full model, we added baseline MD from Cluster 5 as predictors in addition to those demographic characteristics. We used the root mean square error (RMSE) to measure the prediction accuracy – the smaller the RMSE, the better the prediction.

Table 2
AIC, BIC and Log-likelihood values for the Latent Class Analysis.

Model fit indicators	One-cluster model	Two-cluster model	Three-cluster model	Four-cluster model	Five-cluster model	Six-cluster model
AIC	−11777.34	−13943.48	−14609.06	−15092.62	−15387.64	−15638.89
BIC	−11674.01	−13731.08	−14287.59	−14662.07	−14848.01	−14990.20
Log-likelihood	5906.671	7008.741	7360.532	7621.311	7787.819	7932.446

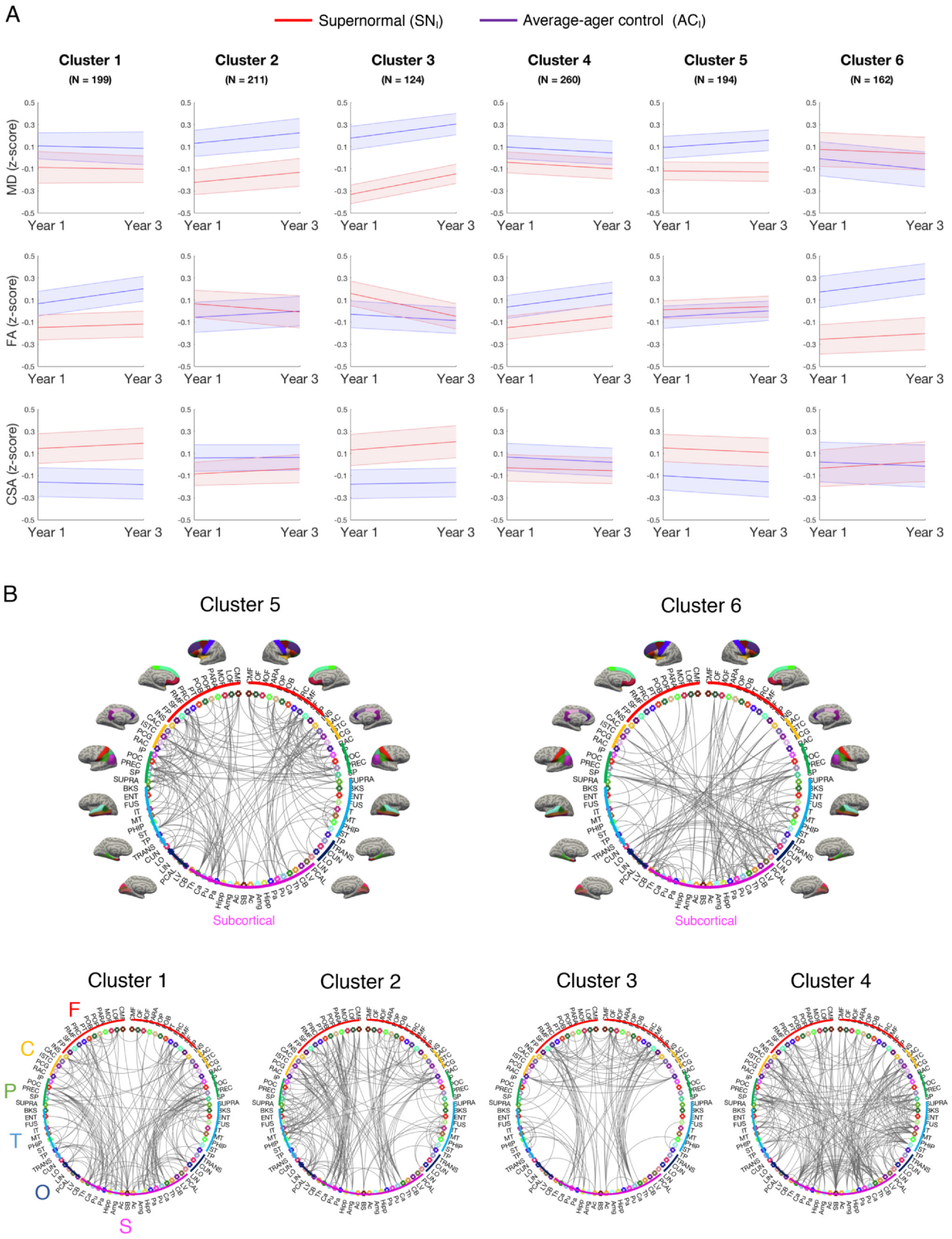

Fig. 2. (A) 2-year trajectories across the WM measures for the 6 clusters in SN_I vs. AC_I. Thick lines indicate mean WM measures of connections for a cluster while shadows indicate standard deviation. (B) Circle plots of connections for the 6 clusters. Nodes are organized in two semicircles from frontal (12o'clock position) to occipital (5o'clock position), and the subcortical regions are presented at the bottom of the circle (6o'clock position). The nodes are colored according to the color lookup table in Freesurfer. Note. MD, mean diffusivity; FA, factional anisotropy; CSA, connected surface area; F, frontal; C, cingulate; P, parietal; T, temporal; O, occipital; S, subcortical. The names and the corresponding abbreviations of nodes can be found in Supplemental table.

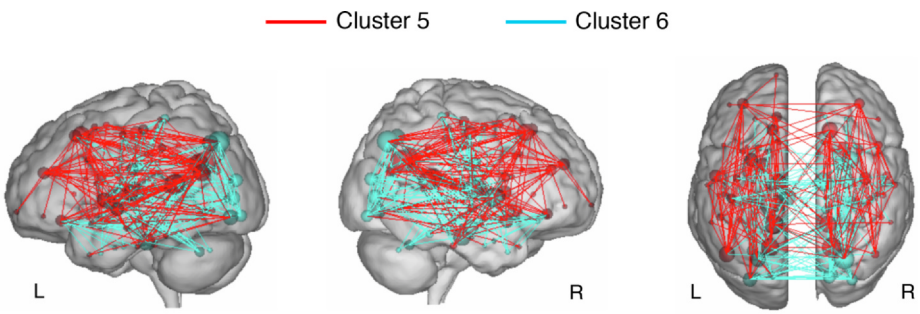

Fig. 3. Glass brain plots of the Cluster 5 and Cluster 6. Note. L, left; R, right.

Let Ψ_f denote the RMSE of the full model and Ψ_b for the baseline model. The prediction improvement of the full model over the baseline model was calculated as $(\Psi_b - \Psi_f)/ \Psi_b$. Adding baseline MD from cluster 5 improved the prediction of CSF Aβ/pTau ratio by 32% (permutation p-value = 0.003) and 21% (permutation p-value = 0.02) for year 1 and year 3, respectively. Structural connectome improved the prediction of AD pathology beyond that of just age, sex and education, which further supports the possibility of Cluster 5 MD values as a "Supernormal structural connectome".

3.3. External validation: Predictive values of the "Supernormal structural connectome" for AD pathology in prodromal AD

Since the most valuable subset of WM connections for predicting AD-related outcomes was the Supernormals' stable connections, MD values of which predict AD pathology, the external validation focused on clinically validating the predictive value of the "Supernormal structural connectome" in separate AD-related context. We used a combined sample (labeled as external/$_E$ sample) of SN_E, AC_E, and aMCI here for the purpose of early detection of the prodromal stage of AD (sample is described in Fig. 1, sample characteristics are presented in Table 1). With SVR and leave-one-out cross validation, MD extracted from the "Supernormal structural connectome" significantly predicted Aβ/pTau ratio (R = 0.529, P < 0.001). Fig. 5**C** presents prediction of Aβ/pTau ratio with MD from the "Supernormal structural connectome" for the external validation cohort. Fig. 5**D** displays the top 30% of the features contributing to predicting Aβ/pTau ratio based on absolute value of coefficients in SVR.

In addition, to ensure the clinical utility of the "Supernormal structural connectome", we also used positive vs. negative AD pathology as the outcome, based on a log-transformed CSF Aβ/pTau ratio of 3.82[37]. With linear support vector machine (SVM) and leave-one-out cross validation, we found the "Supernormal structural connectome" classified participants with positive vs. negative AD pathology significantly above chance (accuracy = 72%, sensitivity = 78%, specificity = 62%, permutation p-value < 0.001). To evaluate the independent contribution of MD of Cluster 5 in classifying AD pathology compared to demographic factors, we also compared a full model to a baseline model where only selective demographic characteristics (i.e., age, sex and education) were used as predictors. Let Ψ_f denote (1-classification accuracy) of the full model and Ψ_b for the baseline model. The prediction improvement of the full model over the baseline model was calculated as $(\Psi_b - \Psi_f)/ \Psi_b$. Adding baseline MD from cluster 5 significantly improved the classification of positive vs. negative AD pathology by 59% (permutation p-value = 0.001).

3.4. Interpretation of the "Supernormal structural connectome"

There are 194 connections within the "Supernormal structural connectome", which involve all lobes and both hemispheres (Fig. 2 Cluster 5 brain map), making the identification of therapeutic targets difficult. We therefore focused on connections within the "Supernormal structural connectome" that were most relevant to AD pathology. Synthesizing the top 30% of connections in the "Supernormal structural connectome" from both internal (Fig. 5**B**) and external (Fig. 5**D**) validations with the largest absolute values of feature weights for AD pathology predictions, we identified a single connection linking the right isthmus cingulate cortex (ISTC) and right precuneus, which showed higher MD for AC ($AC_I + AC_E$) compared to SN ($SN_I + SN_E$) (t(70) = -1.53, P = 0.06) (Fig. 6**A**). Scatterplots of the correlation between the right ISTC-precuneus connection's MD value and AD pathology for the entire sample are presented in Fig. 6**B** (partial correlation R = -0.333, P = 0.001, controlled for age, sex and education; raw R = -0.382, P < 0.001).

Several seemingly contradictory findings were observed: (1) although there was a trend, Supernormals ($SN_I + SN_E$) did not significantly differ from age-matched cognitively normative controls ($AC_I + AC_E$) on AD pathology (F(1,57) = 2.717, P = 0.105, controlled for age, sex and education); (2) Supernormals ($SN_I + SN_E$) had significantly better global cognition (MOCA) than age-matched cognitively normative controls ($AC_I + AC_E$) (F(1,66) = 8.072, P = 0.006, controlled for age, sex and education); (3) the "Supernormal structural connectome" did not directly predict global cognition (Internal validation); and (4) the "Supernormal structural connectome" significantly predicted AD pathology (both internal and external validation). Finally, we investigated mapping the relationships between the "Supernormal structural connectome", AD pathology, and global cognition, combining samples from internal and external validation. For Supernormals ($SN_I + SN_E$), there was a significantly negative relationship between MD in the right ISTC-precuneus and MOCA among individuals with positive AD pathology (partial correlation R_{pc} = -0.885, P = 0.023, controlled for age, sex and education; raw R = -0.699, P = 0.032), but not those with negative AD pathology (Fig. 6**C left**). For age-matched cognitively normative controls ($AC_I + AC_E$) and aMCI, we didn't see this pattern (Fig. 6**C middle and right**). Therefore, the longitudinal stable right ISTC-precuneus connection may protect cognition in SNs with positive AD pathology, which may be a mechanism explaining Supernormals' resistance to AD pathology while maintaining excellent cognition.

4. Discussion

Here we reveal a unique WM structural connectome that is stable and intact for older adults with superior cognition. Baseline MD reliably predicts AD pathology over time using an internal validation sample of cognitively intact individuals, as well as classifies AD pathology using an external validation sample of mixed cognitively intact and abnormal individuals. Within this map, the most distinguishing connection is between the right ISTC and precuneus. Importantly, a significant relationship between the MD of this connection and cognition is only observed among Supernormals with positive, but not negative, AD pathology. We previously identified a stable functional brain map that is unique to Supernormals (Wang et al 2017). The finding of a stable and unique Supernormal structural connectome that is resistant to AD

Table 3
Parameter estimates for Six-cluster model.

		MD				FA				CSA			
		SN_I		AC_I		SN_I		AC_I		SN_I		AC_I	
Cluster	N(%)	Intercept (SE)	Slope (SE)	Intercept (SE)	Slope (SE)	Intercept (SE)	Slope (SE)	Intercept (SE)	Slope (SE)	Intercept(SE)	Slope (SE)	Intercept (SE)	Slope (SE)
1	199(17.3)	−0.08***(0.02)	−0.01 (0.01)	0.12*** (0.02)	−0.01 (0.01)	−0.16*** (0.02)	0.02(0.01)	0.00(0.02)	0.07*** (0.01)	0.12***(0.02)	0.02(0.01)	−0.14***(0.02)	−0.01(0.01)
2	211(18.4)	−0.27***(0.02)	0.05*** (0.01)	0.08*** (0.02)	0.05 *** (0.01)	0.09*** (0.02)	−0.03*** (0.01)	−0.08*** (0.02)	0.03*** (0.01)	−0.10***(0.02)	0.02*(0.01)	0.06**(0.02)	0.00(0.01)
3	124(10.8)	−0.42*** (0.01)	0.09*** (0.01)	0.11*** (0.02)	0.06 *** (0.01)	0.26*** (0.02)	−0.10*** (0.01)	0.00 (0.02)	−0.02* (0.01)	0.09***(0.02)	0.04**(0.01)	−0.18***(0.02)	0.01(0.01)
4	260(22.6)	−0.01 (0.02)	−0.03*** (0.01)	0.12*** (0.01)	−0.03*** (0.01)	−0.20***(0.02)	0.05*** (0.01)	−0.03 (0.02)	0.07*** (0.01)	−0.02(0.02)	−0.01(0.01)	0.09***(0.02)	−0.03**(0.01)
5	194(16.9)	−0.11***(0.01)	−0.01 (0.01)	0.07*** (0.01)	0.03*** (0.01)	0.00(0.01)	0.01(0.01)	−0.08*** (0.02)	0.03*** (0.01)	0.16***(0.02)	−0.02(0.01)	−0.07**(0.02)	−0.03*(0.01)
6	162(14.1)	0.09*** (0.01)	−0.02 (0.01)	0.04(0.02)	−0.05*** (0.01)	−0.29***(0.02)	0.03 *** (0.01)	0.11*** (0.02)	0.06***(0.01)	−0.06(0.03)	0.03(0.01)	0.03(0.02)	−0.02(0.01)

Note: N, number of connections. SE, standard error. Asterisk indicates significance with Bonferroni correction: *, $P < 0.05$; **, $P < 0.01$; and ***, $P < 0.001$.

pathology further strengthens the value of studying biological mechanisms underlying Supernormals for understanding successful cognitive aging.

The WM processing pipeline constructs reliable fiber orientation distribution functions from diffusion MRI data, segments brain tissues, performs anatomy-constrained tractography reconstruction, and extracts connectome matrices (Zhang et al 2018). The Supernormal structural connectome (Cluster 5) contains connections between frontal, cingulate, parietal, temporal, and subcortical regions in the same hemisphere. The subcortical and allocortex regions (e.g., basal ganglia, hippocampus, thalamus, etc.) are critical in transporting neurotransmitters (e.g., dopamine, GABA) to cortical regions. While the specific neurotransmitters participating in the process need to be further determined, the integrity of these cortical-subcortical connections may ensure adaptive neuroplasticity (e.g., rewarding process (Russo & Nestler 2013)) through neurotransmission to resist AD pathology. Also, anterior regions, as well as the connections between anterior and posterior regions, are heavily involved in the Supernormal structural connectome. These characteristics align with previous studies showing Supernormals or Superagers having greater cortical volumes in the anterior regions while stronger functional connections between anterior and posterior regions, compared to average-agers or younger adults (Gefen et al 2015, Harrison et al 2012, Lin et al 2017a, Rogalski et al 2013). Conversely, Cluster 6 (the set with lower MD and higher FA among ACs) engages more interhemispheric connections within the occipital lobe. This phenomenon may be explained by the brain's compensatory sensory enhancement (in this case, visual function), not only functionally, but also microstructurally, in the typical aging process (Cabeza 2002, Reuter-Lorenz & Park 2010). Notably, among a few selected WM integrity measures, the most distinguishable findings in the Supernormal structural connectome are from MD. Previous studies have shown that MD is more sensitive than FA to WM alterations associated with aMCI (Yu et al 2017) and AD (Jin et al 2017), with MD also predicting conversion to dementia (Fellgiebel et al 2006, Müller et al 2007). Physiologically, the absolute diffusion, which is quantified by MD, is a more sensitive marker of neurodegeneration than FA, which simply quantifies the anisotropy of the diffusion tensor (Acosta-Cabronero et al 2010). These results reinforce the elevated relevance of MD in cognitive aging.

Similar to previous studies (Baran & Lin 2018), overall AD pathology did not differ between Supernormals and age-matched cognitively normative controls. However, higher Supernormal structural connectome integrity, especially the lower MD in right ISTC-precuneus connection, is associated with future lower AD pathology. This finding is consistent with previous results showing preservation of posterior cingulate cortex in Superagers compared to typical older adults as well as other critical nodes in the default mode network and salience network (Harrison et al 2018, Sun et al 2016, Zhang et al 2020). Moreover, Supernormals with lower MD in right ISTC-precuneus connection tend to have better cognition, which is only observed in those with positive, but not negative AD pathology. However, such relationships do not exist in age-matched cognitively normative control or aMCI groups. Amyloid plaques deposit on WM connections (esp. axons), disrupting WM integrity (Song et al 2004). While there is no difference in the whole brain average amyloid deposition, our previous cerebral amyloid work coherently revealed that right ISTC is the only region immune to amyloid plaque deposition among Supernormals relative to age-matched cognitively normative older adults (Baran & Lin 2018). Relevantly, these two posterior regions are part of the posterior default mode network, among the first to degenerate in the AD process (Di Paola et al 2010). In addition, the unique function of these two regions, which is not necessarily AD or neurodegeneration related, may also be involved in explaining this phenomenon. ISTC and precuneus are among the very few regions sensitive to different major stressful life events, including chronic stress exposure (Calati et al 2018), psychiatric disorders (e.g., depression, schizophrenia) (Szymkowicz et al 2016,

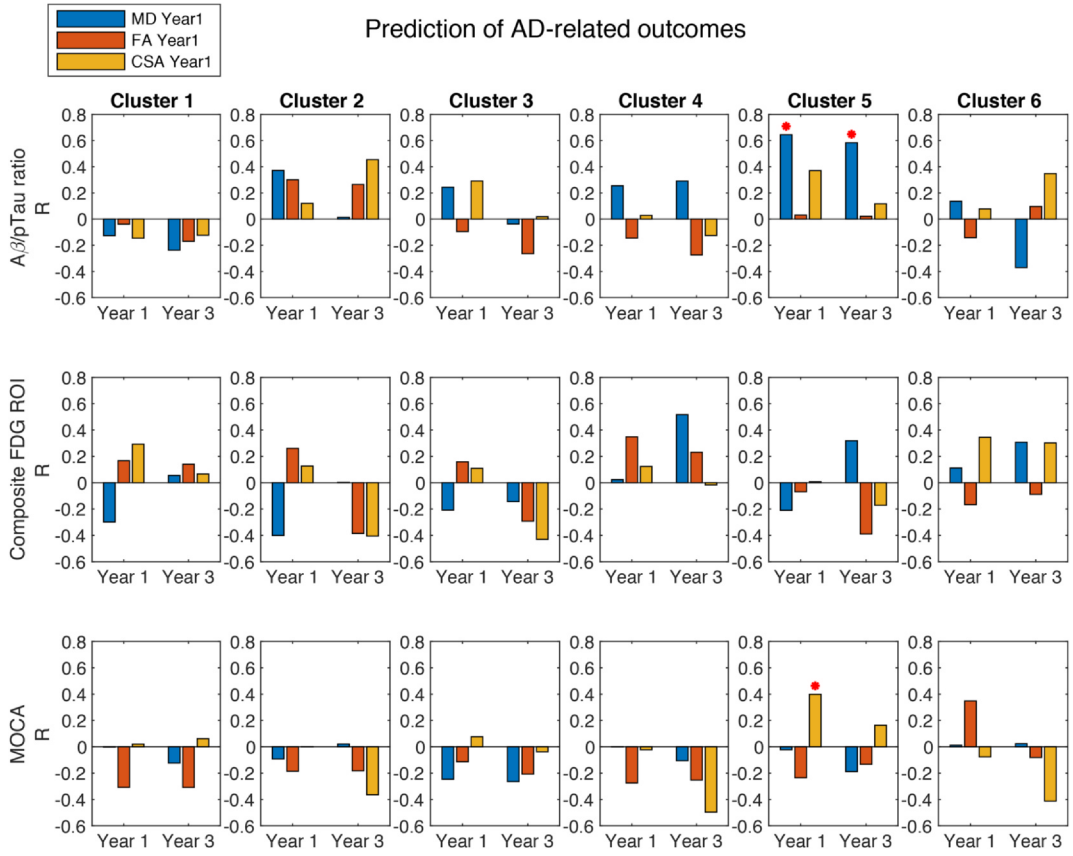

Fig. 4. Outcome predictions using WM measures from the 6 clusters combining the sample of SN_I and AC_I. Red asterisks indicate Bonferroni adjusted statistical significance of $P < 0.05$. (For interpretation of the references to color in this figure legend, the reader is referred to the web version of this article.)

Whitford et al 2014), head trauma (Shin et al 2014), and insomnia (Yu et al 2018). Together, this connection's immunity to amyloid deposition, and/or regulatory capacity over stress/homeostatic regulation may explain Supernormals cognitive excellence despite the similarity in overall AD pathology between Supernormals and cognitively normative older adults.

There is a need for identifying biomarkers for early detection of AD that can simultaneously predict cognitive trajectories and various AD pathologies, and are specific for AD. Existing predictors based on multi-dimensional data at baseline (Bruun et al 2019, Rhodius-Meester et al 2018) are typically focused on clinical progression of dementia and seem to be limited in linking the cognitive and pathological aspects of AD (Giorgio et al 2020). Although an association has been demonstrated between tau and cognitive impairment (Bejanin et al 2017, Riley et al 2002), studies have largely been correlational and have not fully characterized this connection. This gap can be largely explained by the confined focus on understanding risk factors, as opposed to protective factors. Aging populations are often exposed to heterogeneous health conditions that impose secondary adverse effects on cognition or pathologies, which make the revealed risk factors specific for certain conditions or groups of individuals. Studying successful cognitive aging will provide novel insights into the mechanisms involved in protecting cognition against AD pathologies. Enhancing common protective factors such as the Supernormal structural connectome, especially the right ISTC-precuneus connection, may strengthen cognition across different conditions in which risk factors can be too varied to be modified via a common pathway.

5. Next steps and limications

Limitations should be acknowledged. First, of note, consensus on the definition of the cognitively superior ager group is lacking, given inconsistencies in the choice of comparison group or cognitive measures. Superagers are defined as performing at or above average normative values for individuals in their 50 s and 60 s in the memory domain, and within average in non-memory domains (Gefen et al 2015). To differentiate, we use the term Supernormals, given our definition is based on stable and excellent cognition over time. Future studies do need to compare brain profiles between the two definitions to eventually determine whether a unified definition should be used or phenotypes should be developed.

Second, the revealed 194 structural connections in the "Supernormal structural connectome" map helps narrow down the relevant structural connections for predicting cognitive trajectories against AD pathology from approximately 1000 connections, providing a decent set of candidate connections for future validation studies. The study here focuses on identifying a novel brain biomarker. Before moving to determine this map's therapeutic value, the relationship between the "Supernormal structural connectome" and global cognition needs to be further tested in larger samples. This will help further determine whether ISTC-precuneus connection or others from the "supernormal structural connectome" protects global cognition from AD pathology.

In addition, the b-value of 1000 s/mm^2 and the scan resolution of 2.7 mm are not optimal for tractography. Higher signal-to-noise ratio and better spatial resolution with a fairly high b value should be considered in the future studies (Tournier et al 2004, Tournier et al 2008). The current study is focused on the WM integrity indexed by MD, FA and CSA, which do not directly reflect the exact microstructural changes (Delouche et al 2016). Moreover, brain aging is also accompanied by other mechanisms, e.g., decline in grey matter volume and decrease in synapses and level of neurotransmitters. Future studies can

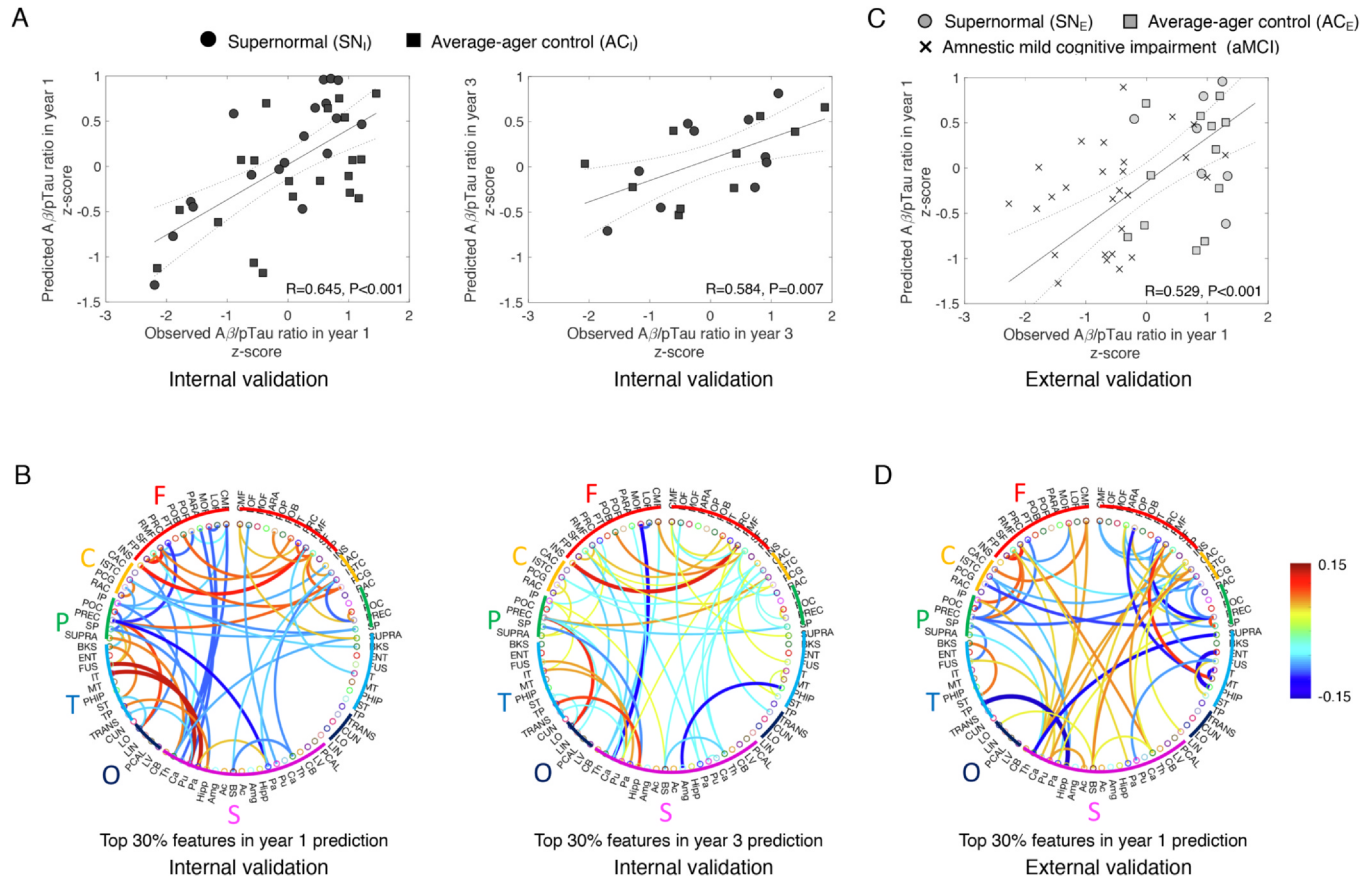

Fig. 5. (A) Scatterplots of prediction of Aβ/pTau ratio using MD from the "Supernormal structural connectome" (Cluster 5) for year 1 and year 3 in Internal validation. (B) The top 30% features (connections) with the largest coefficients in absolute value in predicting Aβ/pTau ratio in Internal validation. (C) Scatterplots of prediction of Aβ/pTau ratio using MD from the "Supernormal structural connectome" 5 in External validation. (D) The top 30% features (connections) with the largest coefficients in absolute value in predicting Aβ/pTau ratio in External validation. Note. The color bar indicates the scale for the feature coefficients. Hot/cold colors indicate positive/negative coefficients.

explore relationships between the supernormal connectome map and these mechanisms.

A critical next step from the current study is to comprehensively examine brain function and structure among Supernormals. Supernormals show longitudinally stable brain function similar to younger adults, most evident by the well-preserved posterior brain regions. Moreover, Supernormals' unique brain function and structure patterns are linked to their cognitive excellence directly (function) or indirectly (structurally via the right ISTC-precuneus connection). This indicates the different, maybe complementary, roles of brain function and structure in supporting excellent cognition. Meanwhile, stress regulation among Supernormals may be an important aspect to further pursue. Our previous study suggests Supernormals have lower oxidative stress burden and inflammation (Mapstone et al 2017). It is unclear if the Supernormal maps, especially the structure and function of the right ISTC-precuneus, are related to these metabolic differences. Lastly, since several studies from our group has been conducted using ADNI, these results should be validated in other datasets to avoid any sample bias.

6. Significance Statement

Cognitive aging is a major public concern. Yet some older adults, known as Supernormals, maintain cognitive superiority. Characterizing the neural profile of Supernormals may help identify therapeutic targets for cognitive aging. Here, studying a longitudinal cohort of Supernormals with a cutting-edge structural connectome processing pipeline, we find a structural connectome-based early biomarker to predict AD progression and explain a potential neural mechanism protecting cognition in the presence of AD pathology.

Funding

Manuscript development was funded by University of Rochester Roberta K. Courtman Revocable Trust fund to Timothy Baran and Zhengwu Zhang, as well as National Institutes of Health (grant number NR015452, AG053193) and University of Rochester Goergen Institute for Data Science Collaborative Pilot Aware Program in Health Analytics and Furth Fund to Feng Lin.

Data collection and sharing for this project was funded by the Alzheimer's Disease Neuroimaging Initiative (ADNI) (National Institutes of Health Grant U01 AG024904) and DOD ADNI (Department of Defense award number W81XWH-12–2-0012). ADNI is funded by the National Institute on Aging, the National Institute of Biomedical Imaging and Bioengineering, and through generous contributions from the following: AbbVie, Alzheimer's Association; Alzheimer's Drug Discovery Foundation; Araclon Biotech; BioClinica, Inc.; Biogen; Bristol-Myers Squibb Company; CereSpir, Inc.; Cogstate; Eisai Inc.; Elan Pharmaceuticals, Inc.; Eli Lilly and Company; EuroImmun; F. Hoffmann-La Roche Ltd and its affiliated company Genentech, Inc.; Fujirebio; GE Healthcare; IXICO Ltd.; Janssen Alzheimer Immunotherapy Research & Development, LLC.; Johnson & Johnson Pharmaceutical Research & Development LLC.; Lumosity; Lundbeck; Merck & Co., Inc.; Meso Scale Diagnostics, LLC.; NeuroRx Research; Neurotrack Technologies; Novartis Pharmaceuticals Corporation; Pfizer Inc.; Piramal Imaging; Servier; Takeda Pharmaceutical Company; and Transition Therapeutics. The Canadian Institutes of Health Research is

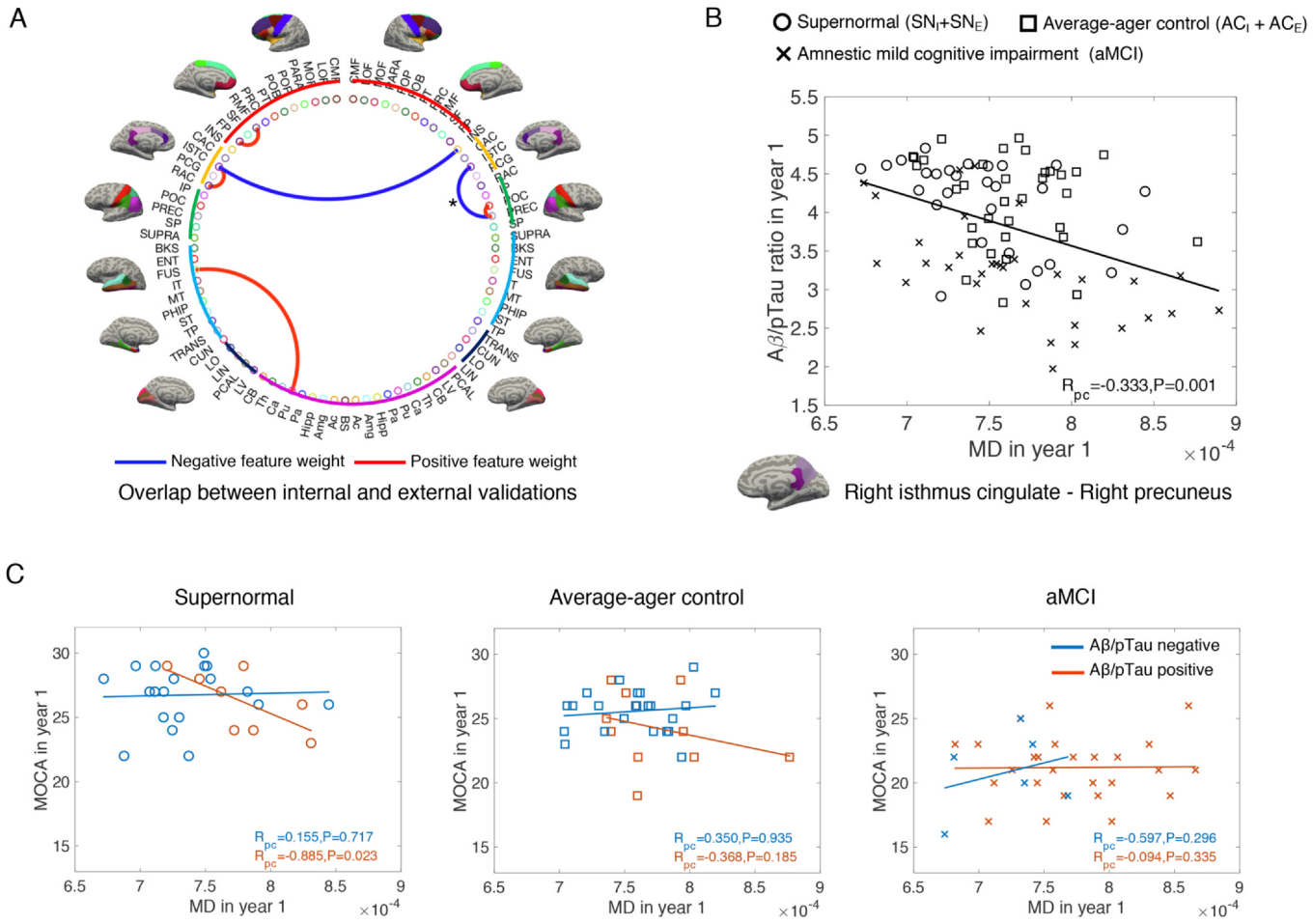

Fig. 6. (A) Overlap of the top 30% of connections in the "Supernormal structural connectome" from both internal and external validations for AD pathology predictions. Asterisk indicates a connection showing higher MD for AC (AC_I + AC_E) compared to SN (SN_I + SN_E). (B) Relationship between right ISTC-precuneus connection MD value and Aβ/pTau ratio for the entire sample, controlled for age, sex and education. (C) Relationship between right ISTC-precuneus connection MD value and MOCA for each group separated by positive or negative AD pathology, controlled for age, sex and education. Note. Different symbols represent different groups: circle, Supernormal (SN_I + SN_E); square: Average-ager control (AC_I + AC_E); cross, aMCI.

providing funds to support ADNI clinical sites in Canada. Private sector contributions are facilitated by the Foundation for the National Institutes of Health (www.fnih.org). The grantee organization is the Northern California Institute for Research and Education, and the study is coordinated by the Alzheimer's Therapeutic Research Institute at the University of Southern California. ADNI data are disseminated by the Laboratory for Neuro Imaging at the University of Southern California.

CRediT authorship contribution statement

Quanjing Chen: Conceptualization, Methodology, Writing - review & editing. **Timothy M. Baran:** Writing - review & editing. **Brian Rooks:** Methodology. **M. Kerry O'Banion:** Writing - review & editing. **Mark Mapstone:** Writing - review & editing. **Zhengwu Zhang:** Methodology, Writing - review & editing. **Feng Lin:** Conceptualization, Supervision, Writing - review & editing. **:** .

Declaration of Competing Interest

The authors declare that they have no known competing financial interests or personal relationships that could have appeared to influence the work reported in this paper.

Appendix A. Supplementary data

Supplementary data to this article can be found online at https://doi.org/10.1016/j.nicl.2020.102413.

References

Acosta-Cabronero, J., Williams, G.B., Pengas, G., Nestor, P.J., 2010. Absolute diffusivities define the landscape of white matter degeneration in Alzheimer's disease. Brain : J. Neurol. 133, 529–539.
Baran, T.M., Lin, F.V., 2018. Amyloid and FDG PET of Successful Cognitive Aging: Global and Cingulate-Specific Differences. J Alzheimers Dis.
Bejanin, A., Schonhaut, D.R., La Joie, R., Kramer, J.H., Baker, S.L., et al., 2017. Tau pathology and neurodegeneration contribute to cognitive impairment in Alzheimer's disease. Brain 140, 3286–3300.
Bozzali, M., Cherubini, A., 2007. Diffusion tensor MRI to investigate dementias: a brief review. Magn Reson Imaging 25, 969–977.
Brickman, A.M., Stern, Y., 2009. In: Aging and Memory in Humans In *Encyclopedia of Neuroscience*. Elsevier, Amsterdam, pp. 175–180.
Bruun, M., Frederiksen, K.S., Rhodius-Meester, H.F., Baroni, M., Gjerum, L., et al., 2019. Impact of a clinical decision support tool on prediction of progression in early-stage dementia: a prospective validation study. Alzheimer's research & therapy 11, 25.
Cabeza, R., 2002. Hemispheric asymmetry reduction in older adults: the HAROLD model. Psychol Aging 17, 85–100.
Calati, R., Maller, J.J., Meslin, C., Lopez-Castroman, J., Ritchie, K., et al., 2018. Repatriation is associated with isthmus cingulate cortex reduction in community-dwelling elderly. The world journal of biological psychiatry : the official journal of the World Federation of Societies of Biological Psychiatry 19, 421–430.
Chang, C.-C., Lin, C.-J., 2011. LIBSVM: a library for support vector machines. ACM transactions on intelligent systems and technology (TIST) 2, 27.
Chua, T.C., Wen, W., Slavin, M.J., Sachdev, P.S., 2008. Diffusion tensor imaging in mild cognitive impairment and Alzheimer's disease: a review. Curr. Opin. Neurol. 21,

83–92.
Crane, P.K., Carle, A., Gibbons, L.E., Insel, P., Mackin, R.S., et al., 2012. Development and assessment of a composite score for memory in the Alzheimer's Disease Neuroimaging Initiative (ADNI). Brain Imaging Behav. 6, 502–516.
Dai, Z., He, Y., 2014. Disrupted structural and functional brain connectomes in mild cognitive impairment and Alzheimer's disease. Neurosci. Bull. 30, 217–232.
Damoiseaux, J.S., Smith, S.M., Witter, M.P., Sanz-Arigita, E.J., Barkhof, F., et al., 2009. White matter tract integrity in aging and Alzheimer's disease. Hum. Brain Mapp. 30, 1051–1059.
Delbeuck, X., Van der Linden, M., Collette, F., 2003. Alzheimer'disease as a disconnection syndrome? Neuropsychol. Rev. 13, 79–92.
Delouche, A., Attye, A., Heck, O., Grand, S., Kastler, A., et al., 2016. Diffusion MRI: Pitfalls, literature review and future directions of research in mild traumatic brain injury. Eur J Radiol 85, 25–30.
Di Paola, M., Spalletta, G., Caltagirone, C., 2010. In vivo structural neuroanatomy of corpus callosum in Alzheimer's disease and mild cognitive impairment using different MRI techniques: a review. J Alzheimers Dis 20, 67–95.
Fellgiebel, A., Dellani, P.R., Greverus, D., Scheurich, A., Stoeter, P., Müller, M.J., 2006. Predicting conversion to dementia in mild cognitive impairment by volumetric and diffusivity measurements of the hippocampus. Psychiatry Res Neuroimaging 146, 283–287.
Fiocco, A.J., Yaffe, K., 2010. Defining successful aging: The importance of including cognitive function over time. Arch. Neurol. 67, 876–880.
Frias, C.M., Lövdén, M., Lindenberger, U., Nilsson, L.-G., 2007. Revisiting the dedifferentiation hypothesis with longitudinal multi-cohort data. Intelligence 35, 381–392.
Gefen, T., Peterson, M., Papastefan, S.T., Martersteck, A., Whitney, K., et al., 2015. Morphometric and histologic substrates of cingulate integrity in elders with exceptional memory capacity. J Neurosci 35, 1781–1791.
Gibbons, L.E., Carle, A.C., Mackin, R.S., Harvey, D., Mukherjee, S., et al., 2012. A composite score for executive functioning, validated in Alzheimer's Disease Neuroimaging Initiative (ADNI) participants with baseline mild cognitive impairment. Brain Imaging Behav. 6, 517–527.
Giorgio, J., Landau, S.M., Jagust, W.J., Tino, P., Kourtzi, Z., 2020. Modelling prognostic trajectories of cognitive decline due to Alzheimer's disease. NeuroImage: Clinical 26, 102199.
Girard, G., Whittingstall, K., Deriche, R., Descoteaux, M., 2014. Towards quantitative connectivity analysis: reducing tractography biases. Neuroimage 98, 266–278.
Hansson, O., Seibyl, J., Stomrud, E., Zetterberg, H., Trojanowski, J.Q., et al., 2018. CSF biomarkers of Alzheimer's disease concord with amyloid-beta PET and predict clinical progression: A study of fully automated immunoassays in BioFINDER and ADNI cohorts. Alzheimers Dement.
Harrison, T.M., Maass, A., Baker, S.L., Jagust, W.J., 2018. Brain morphology, cognition, and beta-amyloid in older adults with superior memory performance. Neurobiol Aging 67, 162–170.
Harrison, T.M., Weintraub, S., Mesulam, M.M., Rogalski, E., 2012. Superior memory and higher cortical volumes in unusually successful cognitive aging. J Int Neuropsychol Soc 18, 1081–1085.
C.-W.-C.-C.-C. Hsu C.-J. Lin A practical guide to support vector classification 2003.
C.R. Jack Jr. M.A. Bernstein N.C. Fox P. Thompson G. Alexander et al. The Alzheimer's Disease Neuroimaging Initiative (ADNI): MRI methods J Magn Reson Imaging 27 2008 685 91.
Jagust, W.J., Bandy, D., Chen, K., Foster, N.L., Landau, S.M., et al., 2010. The Alzheimer's Disease Neuroimaging Initiative positron emission tomography core. Alzheimers Dement 6, 221–229.
Jin, Y., Hueang, C., Daianu, M., Zhan, L., Dennis, E.L., et al., 2017. 3D tract-specific local and global analysis of white matter integrity in Alzheimer's disease. Hum. Brain Mapp. 38, 1191–1207.
Kim, W.H., Racine, A.M., Adluru, N., Hwang, S.J., Blennow, K., et al., 2019. Cerebrospinal fluid biomarkers of neurofibrillary tangles and synaptic dysfunction are associated with longitudinal decline in white matter connectivity: A multi-resolution graph analysis. Neuroimage Clin 21, 101586.
Leisch, F., 2004. FlexMix: A general framework for finite mixture models and latent class regression in R. J. Stat. Softw. 11.
Lim, J.-S., Park, Y.H., Jang, J.-W., Park, S.Y., Kim, S., AsDN, I., 2014. Differential white matter connectivity in early mild cognitive impairment according to CSF biomarkers. PLoS ONE 9, e91400.
Lin, F., Ren, P., Mapstone, M., Meyers, S.P., Porsteinsson, A., et al., 2017a. The cingulate cortex of older adults with excellent memory capacity. Cortex 86, 83–92.
Lin, F.V., Wang, X., Wu, R., Rebok, G.W., Chapman, B.P., Neuroimaging, A.D., I, 2017b. Identification of Successful Cognitive Aging in the Alzheimer's Disease Neuroimaging Initiative Study. J Alzheimers Dis 59, 101–111.
Maier-Hein, K.H., Neher, P.F., Houde, J.C., Cote, M.A., Garyfallidis, E., et al., 2017. The challenge of mapping the human connectome based on diffusion tractography. Nat Commun 8, 1349.
Mapstone, M., Lin, F., Nalls, M.A., Cheema, A.K., Singleton, A.B., et al., 2017. What success can teach us about failure: the plasma metabolome of older adults with superior memory and lessons for Alzheimer's disease. Neurobiol Aging 51, 148–155.
Mayo, C.D., Mazerolle, E.L., Ritchie, L., Fisk, J.D., Gawryluk, J.R., Neuroimaging, Alzheimer's Disease, I, 2017. Longitudinal changes in microstructural white matter metrics in Alzheimer's disease. Neuroimage Clin 13, 330–338.
Medina, D., deToledo-Morrell, L., Urresta, F., Gabrieli, J.D.E., Moseley, M., et al., 2006. White matter changes in mild cognitive impairment and AD: A diffusion tensor imaging study. Neurobiol. Aging 27, 663–672.
Monje, M., 2018. Myelin Plasticity and Nervous System Function. Annu. Rev. Neurosci. 41, 61–76.
Müller, M.J., Greverus, D., Weibrich, C., Dellani, P.R., Scheurich, A., et al., 2007. Diagnostic utility of hippocampal size and mean diffusivity in amnestic MCI. Neurobiol. Aging 28, 398–403.
Nir, T.M., Jahanshad, N., Villalon-Reina, J.E., Toga, A.W., Jack, C.R., et al., 2013. Effectiveness of regional DTI measures in distinguishing Alzheimer's disease, MCI, and normal aging. Neuroimage Clin 3, 180–195.
Nyberg, L., Pudas, S., 2019. Successful memory aging. Annu Rev Psychol 70, 3.1-3.25.
Olshansky, S., 2018. From lifespan to healthspan. JAMA.
Park, D.C., Reuter-Lorenz, P., 2009. The adaptive brain: Aging and neurocognitive scaffolding. Annu Rev Psychol 60, 173–196.
Persson, J., Kalpouzos, G., Nilsson, L.G., Ryberg, M., Nyberg, L., 2011. Preserved hippocampus activation in normal aging as revealed by fMRI. Hippocampus 21, 753–766.
Ram, N., Grimm, K.J., 2009. Growth Mixture Modeling: A Method for Identifying Differences in Longitudinal Change Among Unobserved Groups. Int. J. Behav. Dev. 33, 565–576.
Reuter-Lorenz, P.A., Park, D.C., 2010. Human neuroscience and the aging mind: a new look at old problems. J Gerontol B Psychol Sci Soc Sci 65, 405–415.
Rhodius-Meester, H.F., Liedes, H., Koikkalainen, J., Wolfsgruber, S., Coll-Padros, N., et al., 2018. Computer-assisted prediction of clinical progression in the earliest stages of AD. Alzheimer's & Dementia: Diagnosis, Assessment & Disease Monitoring 10, 726–736.
Riley, K.P., Snowdon, D.A., Markesbery, W.R., 2002. Alzheimer's neurofibrillary pathology and the spectrum of cognitive function: Findings from the Nun Study. Ann. Neurol. 51, 567–577.
Rogalski, E.J., Gefen, T., Shi, J., Samimi, M., Bigio, E., et al., 2013. Youthful memory capacity in old brains: anatomic and genetic clues from the Northwestern SuperAging Project. J Cogn Neurosci 25, 29–36.
Rönnlund, M., Nyberg, L., Bäckman, L., Nilsson, L.-G., 2005. Stability, growth, and decline in adult life span development of declarative memory: Cross-sectional and longitudinal data from a population-based study. Psychol. Aging 20, 3–18.
Rose, S.E., Chen, F., Chalk, J.B., Zelaya, F.O., Strugnell, W.E., et al., 2000. Loss of connectivity in Alzheimer's disease: an evaluation of white matter tract integrity with colour coded MR diffusion tensor imaging. J. Neurol. 69, 528–530.
Rossetti, H.C., Lacritz, L.H., Cullum, C.M., Weiner, M.F., 2011. Normative data for the Montreal Cognitive Assessment (MoCA) in a population-based sample. Neurology 77, 1272–1275.
Russo, S.J., Nestler, E.J., 2013. The brain reward circuitry in mood disorders. Nat Rev Neurosci 14, 609–625.
Schmithorst, V.J., Wilke, M., Dardzinski, B.J., Holland, S.K., 2005. Cognitive functions correlate with white matter architecture in a normal pediatric population: A diffusion tensor MRI study. Hum. Brain Mapp. 26, 139–147.
Seals, D.R., Justice, J.N., LaRocca, T.J., 2016. Physiological geroscience: targeting function to increase healthspan and achieve optimal longevity. The Journal of physiology 594, 2001–2024.
Shaw, L.M., Vanderstichele, H., Knapik-Czajka, M., Clark, C.M., Aisen, P.S., et al., 2009. Cerebrospinal fluid biomarker signature in Alzheimer's disease neuroimaging initiative subjects. Ann Neurol 65, 403–413.
Shen XF, E. S.; Scheinost, D.; Rosenberg, M. D.; Chun, M. M.; Papademetris, X.; Constable, R. T. . 2017. Using connectome-based predictive modeling to predict individual behavior from brain connectivity. Nat Protoc 12: 506–18.
Shin, W., Mahmoud, S.Y., Sakaie, K., Banks, S.J., Lowe, M.J., et al., 2014. Diffusion measures indicate fight exposure-related damage to cerebral white matter in boxers and mixed martial arts fighters. AJNR Am J Neuroradiol 35, 285–290.
Smith, S.M., 2002. Fast robust automated brain extraction. Hum Brain Mapp 17, 143–155.
Song, S.-K., Kim, J.H., Lin, S.-J., Brendza, R.P., Holtzman, D.M., 2004. Diffusion tensor imaging detects age-dependent white matter changes in a transgenic mouse model with amyloid deposition. Neurobiology of Disease 15, 640–647.
Sun, F.W., Stepanovic, M.R., Andreano, J., Barrett, L.F., Touroutoglou, A., Dickerson, B.C., 2016. Youthful Brains in Older Adults: Preserved Neuroanatomy in the Default Mode and Salience Networks Contributes to Youthful Memory in Superaging. J Neurosci 36, 9659–9668.
Szymkowicz, S.M., McLaren, M.E., Kirton, J.W., O'Shea, A., Woods, A.J., et al., 2016. Depressive symptom severity is associated with increased cortical thickness in older adults. Int J Geriatr Psychiatry 31, 325–333.
Tournier, J.D., Calamante, F., Gadian, D.G., Connelly, A., 2004. Direct estimation of the fiber orientation density function from diffusion-weighted MRI data using spherical deconvolution. Neuroimage 23, 1176–1185.
Tournier, J.D., Yeh, C.H., Calamante, F., Cho, K.H., Connelly, A., Lin, C.P., 2008. Resolving crossing fibres using constrained spherical deconvolution: validation using diffusion-weighted imaging phantom data. Neuroimage 42, 617–625.
Voineskos, A.N., Rajji, T.K., Lobaugh, N.J., Miranda, D., Shenton, M.E., et al., 2012. Age-related decline in white matter tract integrity and cognitive performance: A DTI tractography and structural equation modeling study. Neurobiol. Aging 33, 21–34.
Wang, X., Ren, P., Baran, T.M., Raizada, R.D.S., Mapstone, M., et al., 2017. Longitudinal Functional Brain Mapping in Supernormals. Cereb Cortex 1–11.
Whitford, T.J., Lee, S.W., Oh, J.S., de Luis-Garcia, R., Savadjiev, P., et al., 2014. Localized abnormalities in the cingulum bundle in patients with schizophrenia: a Diffusion Tensor tractography study. Neuroimage Clin 5, 93–99.
Yu, J., Lam, C.L.M., Lee, T.M.C., 2017. White matter microstructural abnormalities in amnestic mild cognitive impairment: A meta-analysis of whole-brain and ROI-based studies. Neurosci. Biobehav. Rev. 83, 405–416.
Yu, S., Guo, B., Shen, Z., Wang, Z., Kui, Y., et al., 2018. The imbalanced anterior and posterior default mode network in the primary insomnia. J Psychiatr Res 103, 97–103.
Zhang, J., Andreano, J.M., Dickerson, B.C., Touroutoglou, A., Barrett, L.F., 2020. Stronger Functional Connectivity in the Default Mode and Salience Networks Is Associated With Youthful Memory in Superaging. Cereb Cortex 30, 72–84.
Zhang, Z., Allen, G.I., Zhu, H., Dunson, D., 2019. Tensor network factorizations: Relationships between brain structural connectomes and traits. Neuroimage 197, 330–343.
Zhang, Z., Descoteaux, M., Zhang, J., Girard, G., Chamberland, M., et al., 2018. Mapping population-based structural connectomes. Neuroimage 172, 130–145.